

Methods

Synthesis of ITQ-21 samples

We used precursor gels A (ITQ-21) and B (Al-ITQ-21) with the following compositions. A, 0.33 GeO₂: 0.67 SiO₂: 0.50 MSPTOH: 0.50 HF: 20 H₂O. B, 0.09 GeO₂: 0.91 SiO₂: 0.02 Al₂O₃: 0.50 MSPTOH: 0.50 HF: 3 H₂O. They were prepared by dissolving germanium oxide in the N-methylparietinium hydroxide (MSPTOH) solution. Then, tetraethylorthosilicate and aluminium isopropoxide (for the aluminium-containing sample) were hydrolysed in that solution, and the mixture was mechanically stirred at room temperature until complete elimination of the alcohols had occurred, and the required amount of water until the final composition was reached. Finally, HF was added and the mixture was homogenized.

When the gels were heated at 448 K for five days under conditions of continuous stirring in Teflon-lined stainless-steel autoclaves, the zeolites crystallized. The solids were recovered by filtration, washed with distilled water and dried at 100 °C. Chemical analyses of the ITQ-21 samples presented here are given as Supplementary Information Table 4.

Structure solution and refinement

Powder XRD data were collected at room temperature with a diffractometer (Philips X'Pert) with Bragg-Brentano geometry, and a graphite secondary monochromator. Intensity data were obtained with a fixed divergence slit (1/8°), a maximum illumination length of 10 mm and a goniometer arm of 240 mm, and CuKα_{1,2} radiation (λ = 1.5406, 1.5441 Å). Tube voltage and current were respectively 45 kV and 40 mA. Step scan size and time: 0.02° (2θ) and 9 s. The profile range (2θ) goes from 5.00° to 70.00°. The pattern was indexed according to a cubic F unit cell with a = 27.698 Å, and the analysis of the observed systematic absences led to space group *Fm-3c*.

The crystal structure was solved using XLENS¹⁸ with space group *Fm-3c*, no. 226, that only contains three symmetry independent T sites (T1, T2 and T3). A Rietveld refinement in this cubic symmetry yielded the atomic compositions of sites T1, T2 and T3, and also indicated that the sites containing F⁻ or H₂O/OH⁻ are fully occupied. In space group *Fm-3c*, the cluster shown in Fig. 2 inset is placed at (1/4, 1/4, 1/4), and this site has 43 point group symmetry, so that the Si atoms forming the inner 4MR are averaged over 12 T3 sites. The Rietveld refinement was performed with program LSP7¹⁹ yielding the atomic coordinates listed in Supplementary Information Table 1. Number of contributing reflections is 224; number of geometric restraints of type d(T-O) is 12 (for T1: 1.69(3) Å; T2: 1.66(3); T3: 1.61(3)). Interatomic distances of type O-T-O were also used as restraints with a standard deviation of 0.06 Å. Number of structural parameters: 23. Number of profile parameters: 7, including zero shift (0.029° 2θ) with visually estimated background. Profile function: Pearson-VII. Rietveld overall thermal coefficient: B = 2.9 Å². The residuals of the refinement were: R_{wp} = 0.083; R_p = 0.063, R₁ = 0.127. The good fit between observed and calculated patterns can be seen in Fig. 1.

Also, the possibility that all clusters are equally oriented has been checked by assuming the tetragonal space group *I4/mcm* no. 140 (a_T ≈ a/√2, c_T ≈ a). In spite of the much larger number of parameters involved (50), the improvement of the residuals is minimal. In addition, if the topology were tetragonal, the structure along the c axis would be significantly different from that along the a axis, and this should be evident in the cell parameters. However, the refined tetragonal parameters a_T = 19.5896(10) and c_T = 27.6946(33) Å correspond, within the statistical error, to the cubic cell. Nevertheless, a tetragonal structure cannot be completely ruled out, as the presence of twinned crystals with ordered domains would also result in cubic cell parameters, despite the tetragonal structure. High-resolution electron microscopy investigations might help to clarify this aspect of the ITQ-21 structure.

Catalytic tests

The catalytic experiments were performed in a Microactivity Test Unit (ASTM D-3907). Product determination, including a detailed analysis of the gasoline fraction—PIONA (gas chromatographic analysis of paraffins, isoparaffins, olefins, naphthenes and aromatic hydrocarbon types in gasoline), RON and MON numbers—were performed as described²⁰. Zeolites were pelletized, crushed and sieved, and 0.50 g of the 0.59–0.84-mm fraction was taken and diluted in 2.50 g of inert silica. In the case of the USY/ZSM-5 mixture, they were placed in consecutive beds as described previously²¹. The catalyst/oil ratio was calculated by dividing the amount of zeolite by the amount of gas oil fed.

Received 2 October 2001; accepted 18 June 2002; doi:10.1038/nature00924.

1. Marilly, C. Evolution of refining and petrochemicals. What is the place of zeolites? *Stud. Surf. Sci. Catal.* **135**, 37–60 (2001).
2. Biswas, J. & Maxwell, I. E. Recent process-related and catalyst-related developments in fluid catalytic cracking. *Appl. Catal.* **63**, 197–258 (1990).
3. Martino, G. Catalysis for oil refining and petrochemistry, recent developments and future trends. *Stud. Surf. Sci. Catal.* **A 130**, 83–103 (2000).
4. Freyhardt, C. C., Tsapatsis, M., Lobo, R. F., Balkus, K. J. Jr & Davis, M. E. A high-silica zeolite with a 14-tetrahedral-atom pore opening. *Nature* **381**, 295–298 (1996).
5. Yoshikawa, M. *et al.* Synthesis, characterization, and structure solution of CIT-5, a new, high-silica, extra-large-pore molecular sieve. *J. Phys. Chem. B* **102**, 7139–7147 (1998).
6. Treacy, M. M. J. & Newsam, J. M. Two new three-dimensional twelve-ring zeolite frameworks of which zeolite beta is a disordered intergrowth. *Nature* **332**, 249–251 (1988).
7. Cambor, M. A. *et al.* High silica zeolites with three-dimensional systems of large pore channels. *Micropor. Mesopor. Mater.* **48**, 11–22 (2001).
8. Corma, A., Navarro, M. T., Rey, F., Rius, J. & Valencia, S. Pure polymorph C of zeolite beta synthesized by using framework isomorphous substitution as a structure-directing mechanism. *Angew. Chem. Int. Edn Engl.* **40**, 2277–2280 (2001).
9. Baerlocher, Ch., Meier, W. M. & Olson, D. H. *Atlas of Zeolite Framework Types* 5th edn (Elsevier, Amsterdam, 2000).

10. O'Keeffe, M. & Yaghi, O. M. Germanate zeolites: contrasting the behaviour of germanate and silicate structures built from cubic T₈O₂₀ units (T = Ge or Si). *Chem. Eur. J.* **5**, 2796–2801 (1999).
11. Corma, A., Navarro, M. T., Rey, F. & Valencia, S. Synthesis of pure polymorph C of beta zeolite in a fluoride-free system. *Chem. Commun.* **16**, 1486–1487 (2001).
12. Corma, A., Diaz-Cabanas, M. J. & Fornes, V. Synthesis, characterization, and catalytic activity of a large-pore tridirectional zeolite, H-ITQ-7. *Angew. Chem. Int. Edn Engl.* **39**, 2346–2349 (2000).
13. Blasco, T. *et al.* Preferential location of Ge in the double four-membered ring units of ITQ-7 zeolite. *J. Phys. Chem. B* **106**, 2634–2642 (2002).
14. Klinowski, J. Nuclear magnetic resonance of zeolites. *Prog. Nucl. Magn. Reson. Spectrosc.* **16**, 237–309 (1984).
15. Cerqueira, H. S., Mihindou-Koumba, P. C., Magnoux, P. & Guisnet, M. Methylcyclohexane transformation over HFAU, HBEA, and HMF1 zeolites: I. Reaction scheme and mechanisms. *Ind. Eng. Chem. Res.* **40**, 1032–1041 (2001).
16. Corma, A. *et al.* Methylcyclohexane and meyoethylcyclohexene cracking over zeolite Y catalysts. *Appl. Catal.* **67**, 307–324 (1991).
17. Lacombe, S., Patrigeon, A. & Benazzi, E. n-heptane hydroconversion and methylcyclohexane cracking as model reactions to investigate the pore topology of NU-88 zeolite. *Stud. Surf. Sci. Catal.* **135**, 4272–4279 (2001).
18. Rius, J. XLENS, a direct methods program based on the modulus sum function: Its application to powder data. *Powder Diffraction* **14**, 267–273 (1999).
19. Rius, J. Program LSP7. A program for restrained Rietveld refinement (Institut de Ciència de Materials de Barcelona-CSIC, 1999).
20. Corma, A., Martínez-Triguero, J. & Martínez, C. The use of ITQ-7 as a FCC zeolitic additive. *J. Catal.* **197**, 151–159 (2001).
21. Corma, A. & Martínez-Triguero, J. The use of MCM-22 as a cracking zeolitic additive for FCC. *J. Catal.* **165**, 102–120 (1997).

Supplementary Information accompanies the paper on Nature's website (<http://www.nature.com/nature>).

Acknowledgements

We thank J. L. Jordá for partial analyses for the structure determination and for discussions. J.R. thanks the "D. Gral de Investigación" of the MCYT for support. This work was supported by the CICYT.

Competing interests statement

The authors declare that they have no competing financial interests.

Correspondence and requests for materials should be addressed to A.C. (e-mail: acorma@itq.upv.es).

Lamellar magnetism in the haematite–ilmenite series as an explanation for strong remanent magnetization

Peter Robinson*†, Richard J. Harrison‡, Suzanne A. McEnroe*† & Robert B. Hargraves§

* Geological Survey of Norway, N-7491, Trondheim, Norway
 † Department of Geosciences, University of Massachusetts, Amherst, Massachusetts 01003, USA
 ‡ Department of Earth Sciences, University of Cambridge, Cambridge, UK
 § Department of Geosciences, Princeton University, Princeton, New Jersey 08544, USA

Magnetic anomalies associated with slowly cooled igneous and metamorphic rocks are commonly attributed to the presence of the mineral magnetite. Although the intermediate members of the ilmenite–haematite mineral series can also carry a strong ferrimagnetic remanence¹, it is preserved only in rapidly cooled volcanic rocks, where formation of intergrowths of weakly magnetic haematite and paramagnetic ilmenite is suppressed. But the occurrence of unusually large and stable magnetic remanence in rocks containing such intergrowths has been known for decades^{2–5}, and has recently been the subject of intense investigation^{6–10}. These unmixed oxide phases have been shown

to contain pervasive exsolution lamellae with thickness from 100 μm down to about 1 nm (one unit cell). These rocks, many of which contain only a few per cent of such oxides, show natural remanent magnetizations up to 30 A m^{-1} —too strong to be explained even by pure haematite in an unsaturated state^{11,12}. Here we propose a new ferrimagnetic substructure created by ferrous–ferric ‘contact layers’ that reduce charge imbalance along lamellar contacts between antiferromagnetic haematite and paramagnetic ilmenite. We estimate that such a lamellar magnetic material can have a saturation magnetization up to 55 kA m^{-1} —22 times stronger than pure haematite—while retaining the high coercivity and thermal properties of single-domain haematite.

Slowly cooled rocks from New York⁶, Sweden⁷ and Norway^{8–10}, containing finely exsolved members of the haematite–ilmenite (Fe_2O_3 – FeTiO_3) series, have strong and extremely stable remanent magnetization, suggesting an explanation for some magnetic anomalies in the deep Earth and on planetary bodies that no longer retain a magnetic field, such as Mars. Common to these rocks are grains of ilmenite–haematite containing multiple generations of exsolution lamellae, with thickness ranging down to unit-cell scale (1–2 nm; Fig. 1). These were magnetized about one billion years ago, and are magnetically extremely ‘hard’ (many do not demagnetize in alternating fields of 0.1 T, the typical maximum alternating field used in palaeomagnetic laboratories). Thermal experiments show that demagnetization occurs between 530 °C and 650 °C, comparable to, or higher than, near-endmember magnetite, and consistent with slightly titanian haematite. Haemo-ilmenite samples without coexisting magnetite have natural remanent magnetization to magnetic saturation ratios of only ~2.5%, showing that the haematite component is in an unsaturated state. These observations led to a theoretically unexplained but firm conviction that the magnetic remanence of these materials relates to the abundance of exsolution lamellae produced during slow cooling, and is strongly coupled to

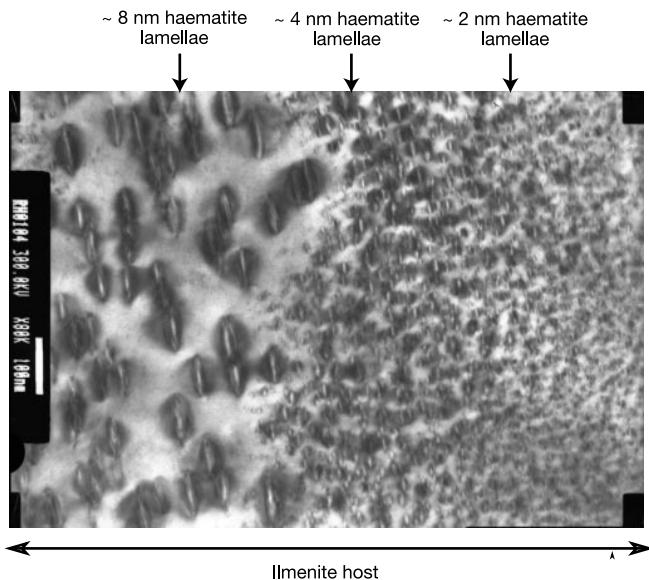


Figure 1 Transmission electron microscope image of haematite exsolution lamellae parallel to (001) in an ilmenite host from South Rogaland, Norway. Three thickness classes (from left to right) of about 8 nm, 4 nm and 2 nm are shown, interpreted as the result of three generations of lamellar nucleation and growth with slowly falling temperature. White scale bar, 100 nm. Dark fringes around lamellae indicate lattice strain in the host adjacent to coherent lamellar boundaries, postulated to increase magnetic coercivity¹⁸.

the antiferromagnetic sublattice of the haematite lamellae^{7,8,13}. Despite extensive study, the magnetic properties of these rocks could not be reconciled with their magnetic petrology using conventional rock-magnetic theory, and required a new departure.

The crystal structures of ilmenite and haematite consist of stacked cation layers^{14,15}. The magnetic moments on alternating layers (referred to as α and β) align antiparallel to each other. The net magnetic moment of the structure is given by the difference between the α and β sublattice magnetizations, which in turn is determined by the partitioning of Fe^{2+} , Fe^{3+} and Ti between the layers. In pure haematite, both α and β are occupied by Fe^{3+} , resulting in an antiferromagnetic structure with zero net moment (in reality, the antiparallel alignment is slightly canted, leading to a small parasitic moment perpendicular to the alignment of the spins). In haematite-rich titanohaematite, Fe^{2+} , Fe^{3+} and Ti are randomly distributed over α and β , again leading to an antiferromagnetic structure with zero net moment. In ilmenite-rich ferri-ilmenite, layers containing mixtures of Fe^{2+} and Fe^{3+} alternate with layers containing mixtures of Ti and Fe^{3+} . The unequal distribution of Fe leads to a net ferrimagnetic moment. Because of the high Ti content, however,

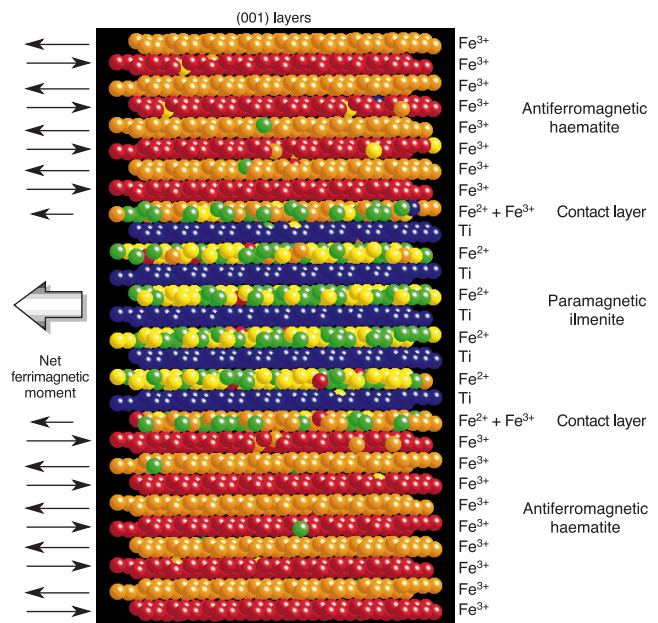


Figure 2 Part of a Monte Carlo simulation of cation ordering, magnetic ordering, and exsolution in the ilmenite–haematite system. 28 layers of a 40-layer cell are shown. Simulation was performed at 500 K and bulk composition 25 mol% ilmenite (Ilm₂₅). During the simulation, the chemical and magnetic interactions between cations and spins are modelled using pair interaction energies out to third nearest neighbours. The distribution of the cations and orientations of their magnetic moments (either left or right in this case) are varied until thermodynamic equilibrium is achieved (that is, the free energy is minimized). Instantaneous snapshots of the equilibrium structure can then be examined. Cations are coloured according to chemistry and orientation of magnetic moment (red, Fe^{3+} , moment $5 \mu_B$ pointing right; orange, Fe^{3+} , moment $5 \mu_B$ pointing left; yellow, Fe^{2+} , moment $4 \mu_B$ pointing right; green, Fe^{2+} , moment $4 \mu_B$ pointing left; blue, Ti with no moment). Upper and lower parts of figure correspond to essentially pure antiferromagnetic haematite (alternating Fe^{3+} layers with left and right spins). In the centre is a lamella of essentially pure paramagnetic ilmenite (Ti layers alternating with layers containing equal numbers of Fe^{2+} -spin left and Fe^{2+} -spin right). Layers at interfaces between ilmenite and haematite contain a mixture of Fe^{2+} and Fe^{3+} . They do not correspond to the chemistry of either haematite or ilmenite, and are called ‘contact layers’. They were observed in all simulations performed within the low-temperature antiferromagnetic haematite + paramagnetic ilmenite stability field.

ferrimagnetic ferri-ilmenites have low Curie temperatures, and are paramagnetic above room temperature.

According to the above description, exsolution intergrowths of titanohaematite and ferri-ilmenite, such as those depicted in Fig. 1, contain an antiferromagnetic phase (with small canted moment) and a paramagnetic phase, neither of which has the correct combination of properties to explain the strong remanence observed in these materials. To determine the source of magnetization in these fine-scale intergrowths, an atomistic simulation of cation ordering, magnetic ordering, and exsolution in the ilmenite–haematite solid solution was performed, using the Monte Carlo method^{14,15}. Figure 2 shows a small section of a Monte Carlo simulation cell performed at 500 K and a bulk composition of 25 mol% ilmenite (Ilm₂₅). The upper and lower parts of Fig. 2 correspond to essentially pure antiferromagnetic haematite (layers of Fe³⁺ with alternating left and right spins). In the centre is a lamella of essentially pure paramagnetic ilmenite (layers of Ti alternating with layers containing equal numbers of Fe²⁺-spin left and Fe²⁺-spin right). The cation layers at the interface between ilmenite and haematite contain a mixture of Fe²⁺ and Fe³⁺. These layers do not correspond to the chemistry of either haematite or ilmenite, and are referred to as ‘contact’ layers. They improve, though not perfectly, local Pauling bond-strength satisfaction of oxygen in layers parallel to (001).

The presence of contact layers creates an imbalance between the equal and opposite α and β sublattice magnetizations of the antiferromagnetic haematite host. This imbalance generates a net ferrimagnetic moment, which necessarily adopts both the coercivity and thermal stability of the haematite host. This concept is best illustrated using simplified layer models (Fig. 3). Figure 3a and b

illustrates an antiferromagnetic host of composition Ilm₁₄ containing two paramagnetic ilmenite lamellae of composition Ilm₈₃. These compositions were chosen to represent possible low-temperature equilibrium states according to the calculated phase diagram¹⁶. The haematite host is antiferromagnetic, containing an equal number of left and right magnetic moments. Insertion of the lower ilmenite lamella removes an odd number of haematite layers, creating a net moment equivalent to the sublattice magnetization of a single haematite layer (M_{haem}), pointing to the right. The sublattice magnetizations of the two contact layers (M_{con}) are antiferromagnetically coupled to the haematite host, creating a magnetic moment of $2M_{\text{con}}$, pointing to the left. The end result is a net ferrimagnetic moment for the lamella of $2M_{\text{con}} - M_{\text{haem}}$, pointing to the left (large arrow).

The orientation of the moment associated with each lamella depends on its vertical position when nucleated. In Fig. 3a, the upper lamella is magnetically in-phase with the lower one, and the moments are additive. For the compositions shown, a net ferrimagnetic moment of $0.28 \mu_B$ per formula unit (p.f.u.) (where μ_B is the Bohr magneton) is achieved. In Fig. 3b, the upper lamella is magnetically out-of-phase with the lower one, and the moments cancel.

Figure 3c and d illustrates a paramagnetic host of composition Ilm_{89.7} containing two haematite precipitates of composition Ilm₆. Lamellae in Fig. 3c and d occupy identical positions, dictated by the surrounding ilmenite (that is, each haematite lamella must be initiated on a former Ti layer of the ilmenite host). In Fig. 3c, the moment of the upper lamella is parallel to the lower one, whereas in Fig. 3d it is antiparallel. Thus, the orientation of the moments

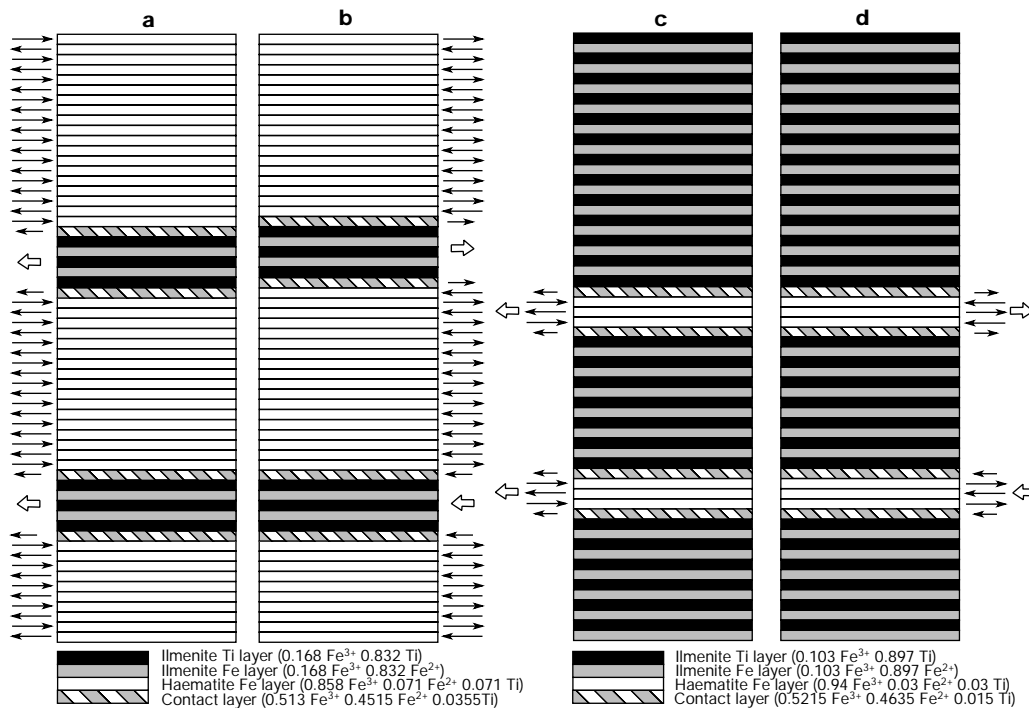


Figure 3 Models of multilayer lamellar magnetism. Panels **a** and **b** show haematite hosts, **c** and **d** show ilmenite hosts. Dark arrows indicate the direction and relative magnitude of magnetic moments in each cation layer. Open arrows indicate the direction of net moment for each lamella ($4.168 \mu_B$ in **a** and **b**; $4.103 \mu_B$ in **c** and **d**). **a, b**, 60 layers in a 20/80 ratio of paramagnetic ilmenite (Ilm_{83.2}) and antiferromagnetic haematite (Ilm_{14.2}). Each contains two ilmenite lamellae, one unit cell thick. In **a**, the moments of the two lamellae are in-phase with each other and the net moment is $(2 \times 4.168)/30 = 0.278 \mu_B$ p.f.u. In **b**, the moments of the two lamellae are out-of-phase with each other, and the net moment

is zero. Physical positioning of an ilmenite lamella determines the direction, left or right, of its net moment within an antiferromagnetic haematite host. **c, d**, 100 layers in a 92/8 ratio of ilmenite (Ilm_{89.7}) and haematite (Ilm_{6.0}). Bottoms of models have been cut to save space. Each contains two haematite lamellae, two-thirds of a unit cell thick. For **c**, the net moment of the upper lamella points to the left, whereas in **d** it points to the right. For **c**, the net moment is $(2 \times 4.103 \mu_B)/50 = 0.164 \mu_B$ p.f.u. For **d**, the net moment is zero.

associated with haematite lamellae in an ilmenite host are not related to their physical placement, as is the case for ilmenite lamellae in a haematite host (Fig. 3a and b). For the compositions shown, the net moment in Fig. 3c is $0.164 \mu_B$ p.f.u. The differences between haematite and ilmenite hosts in Fig. 3 reflect variations in coercivity. Demagnetization in ilmenite requires only demagnetization of haematite lamellae; in haematite, the entire host must be demagnetized.

Natural haematite and ilmenite hosts should contain combinations of in-phase and out-of-phase lamellae. No crystallographic feature favours in-phase over out-of-phase nucleation, but there is a natural condition favouring in-phase lamellae. When (001) planes of haematite or ilmenite are parallel to the magnetic field at nucleation, the field will strongly favour nucleation of in-phase lamellae, and strong remanence in (001). In a haematite host, this implies that the field actually determines the physical placement of the nucleating ilmenite lamellae. In an ilmenite host, however, the field only determines the magnetic orientation of haematite lamellae; physical position is dictated by chemistry. When (001) planes are normal to the field, or in the absence of a field, a random distribution of in- and out-of-phase lamellae results, producing zero net magnetization.

The intensity of lamellar magnetism is strongest when (1) the proportion of exsolved lamellar material is large, (2) lamellae are of minimal size and maximum abundance, maximizing the surface area of contact layers, and (3) host (001) planes are parallel to the magnetizing field, promoting in-phase magnetization. In favourable natural circumstances, a saturated magnetic moment of $0.3 \mu_B$ p.f.u. might be achieved with magnetic moments of all lamellae in-phase and aligned, corresponding to 55 kA m^{-1} , which may be compared to 480 kA m^{-1} for pure magnetite and 2.5 kA m^{-1} (ref. 15) for pure spin-canted antiferromagnetic haematite. Thus, a magnetization 22 times larger than pure haematite is achievable, while retaining the high coercivity and thermal stability of single-domain haematite. A rock containing 1% of similar material, but with only 6% of lamellae magnetically in phase, would have a magnetization of 33 A m^{-1} .

Kletetschka *et al.*¹⁷ have an alternative explanation for the strong and stable remanence of titanohaematite in haemo-ilmenite. They claim early formation, during cooling, of coarse antiferromagnetic haematite lamellae, which are multidomain and hence, according to these authors, capable of acquiring strong thermal remanent magnetization, which is merely 'hardened' by later exsolution. This would have a spin-canted magnetization perpendicular to the lamellar magnetic moment proposed here. However, in our interpretation of the phase diagrams^{15,16}, the only permissible coarse titanohaematite lamellae would be paramagnetic (magnetically disordered) during their formation, only becoming magnetized on cooling below 390°C (ref. 15) as they break down to a fine intergrowth of ordered antiferromagnetic haematite and cation-ordered ilmenite, qualitatively like the pattern illustrated in Fig. 3a. This low exsolution temperature shows that the magnetization is a chemical remanence, not a thermal remanent magnetization, because formation of the antiferromagnetic haematite takes place $100\text{--}200^\circ\text{C}$ below its Néel temperature.

Lamellar magnetism, with its 'hard' magnetic memory, is responsible for many remanence-dominated anomalies over ancient Earth rocks, and is a possible source for some deep-crustal magnetic anomalies on Earth or on planets such as Mars that once had a magnetic field. We believe that lamellar magnetism could also provide the basis for development of a highly stable magnetic storage unit. □

Received 17 May; accepted 26 June 2002; doi:10.1038/nature00942.

- Ishikawa, Y. & Akimoto, S. Magnetic property and crystal chemistry of ilmenite (MeTiO_3) and hematite ($\alpha\text{Fe}_2\text{O}_3$) system II. Magnetic property. *J. Phys. Soc. Jpn* **13**, 1298–1310 (1958).
- Balsley, J. R. & Buddington, A. F. Iron titanium oxide minerals, rocks, and aeromagnetic anomalies of

- the Adirondack area, New York. *Econ. Geol.* **53**, 777–805 (1958).
- Hargraves, R. B. Magnetic anisotropy and remanent magnetism in hemo-ilmenite ore deposits at Allard Lake, Quebec. *J. Geophys. Res.* **64**, 1565–1578 (1959).
- Carmichael, C. M. The magnetic properties of ilmenite-hematite crystals. *Proc. R. Soc. Lond. A* **263**, 508–530 (1961).
- Merrill, R. T. & Grommé, C. S. Nonreproducible self-reversal of magnetization in diorite. *J. Geophys. Res.* **74**, 2014–2024 (1969).
- McEnroe, S. A. & Brown, L. L. A closer look at remanence-dominated aeromagnetic anomalies: Rock-magnetic properties and magnetic mineralogy of the Russell Belt microcline-sillimanite gneiss, northwest Adirondack Mountains, New York. *J. Geophys. Res.* **105**, 16437–16456 (2000).
- McEnroe, S. A., Harrison, R. J., Robinson, P., Golla, U. & Jercinovic, M. J. Effect of fine-scale microstructures in titanohaematite on the acquisition and stability of natural remanent magnetization in granulite-facies metamorphic rocks southwest Sweden: Implications for crustal magnetism. *J. Geophys. Res.* **106**, 30523–30546 (2001).
- McEnroe, S. A., Robinson, P. & Panish, P. T. Detailed chemical and petrographic characterization of ilmenite- and magnetic-rich cumulates of the Sokndal region, Rogaland, Norway. *Norweg. Geol. Surv. Bull.* **436**, 49–56 (2000).
- McEnroe, S. A., Robinson, P. & Panish, P. T. Aeromagnetic anomalies, magnetic petrology and characterization of ilmenite- and magnetic-rich cumulates of the Sokndal region, Rogaland, Norway. *Am. Mineral.* **86**, 1447–1468 (2001).
- Robinson, P., Panish, P. T. & McEnroe, S. A. Minor element chemistry of hemo-ilmenite- and magnetite-rich cumulates from the Sokndal region, south Rogaland, Norway. *Am. Mineral.* **86**, 1469–1476 (2001).
- Banerjee, S. K. Magnetic properties of Fe-Ti oxides. *Rev. Mineral.* **25**, 107–128 (1991).
- Dunlop, D. J. & Özdemir, O. *Rock Magnetism: Fundamentals and Frontiers* (Cambridge Univ. Press, New York, 1997).
- McEnroe, S. A., Robinson, P. & Panish, P. T. Correlation between oxide mineralogy, rock-magnetic properties and aeromagnetic anomalies: Case study from the Sokndal Region, South Norway. *Eos* **79**, S362 (1998).
- Harrison, R. J. Magnetic transitions in minerals. *Rev. Mineral.* **39**, 175–202 (2000).
- Harrison, R. J. & Becker, U. in *Solid Solutions in Silicate and Oxide Systems* (ed. Geiger, C. A.) Vol. 3, 349–383 (Notes in Mineralogy, European Mineralogical Union, Eötvös Univ. Press, Budapest, 2001).
- Burton, B. P. The interplay of chemical and magnetic ordering. *Rev. Mineral.* **25**, 303–321 (1991).
- Kletetschka, G., Wasilewski, P. J. & Taylor, P. T. The role of hematite-ilmenite solid solution in the production of magnetic anomalies in ground and satellite-based data. *Tectonophysics* **347**, 166–177 (2002).
- Merrill, R. T. A possible source for the coercivity of ilmenite-hematite minerals. *J. Geomag. Electr.* **20**, 181–185 (1968).

Acknowledgements

TEM imaging and TEM analytical studies at Institut für Mineralogie, Universität Münster, were done in cooperation with A. Putnis and U. Golla, and atomic simulations were carried out in cooperation with U. Becker. Electron microprobe studies at Univ. Massachusetts were completed with assistance from P.T. Panish and M.J. Jercinovic. S.A.M. and P.R. were supported by the strategic research fund of the Geological Survey of Norway and Bayerisches Geo-Institut. The work of S.A.M. on Swedish granulites was initiated during a Fellowship from the American-Scandinavian Foundation and from the Institute of Rock Magnetism, and her work in the Adirondacks was supported by the NSF. R.J.H. carried out his studies while a research fellow at the Institut für Mineralogie, Universität Münster.

Competing interests statement

The authors declare that they have no competing financial interests.

Correspondence and requests for materials should be addressed to P.R. (e-mail: peter.robinson@ngu.no).

A 20-km-diameter multi-ringed impact structure in the North Sea

Simon A. Stewart* & Philip J. Allen†

* BP plc, Burnside Road, Dyce, Aberdeen AB21 7PB, UK
 † Production Geoscience Ltd, Banchory AB31 5YR, UK

Most craters found on Earth are highly eroded, poorly preserved and only exposed on land^{1,2}. Here we describe a multi-ringed impact structure discovered in the North Sea from the analysis of three-dimensional seismic reflection data. The structure is 20 km in diameter, and has at least ten distinctive concentric rings located between 2 and 10 km from the crater centre. The